



ELSEVIER

Contents lists available at ScienceDirect

Applied Surface Science

journal homepage: [www.elsevier.com/locate/apsusc](http://www.elsevier.com/locate/apsusc)

Full Length Article

# Formation of SnO and SnO<sub>2</sub> phases during the annealing of SnO(x) films obtained by molecular beam epitaxy

Alexander Nikiforov<sup>a,b,\*</sup>, Vyacheslav Timofeev<sup>a</sup>, Vladimir Mashanov<sup>a</sup>, Ivan Azarov<sup>a,e</sup>,  
Ivan Loshkarev<sup>a</sup>, Vladimir Volodin<sup>a,e</sup>, Dmitry Gulyaev<sup>a</sup>, Igor Chetyrin<sup>c</sup>, Ilya Korolkov<sup>d,e</sup>

<sup>a</sup> A.V. Rzhanov Institute of Semiconductor Physics SB RAS, 13 Lavrentyev Avenue, Novosibirsk 630090, Russia

<sup>b</sup> National Research Tomsk State University, 36 Lenin Avenue, Tomsk 634050, Russia

<sup>c</sup> Borekov Institute of Catalysis SB RAS, 5 Lavrentyev Avenue, Novosibirsk 630090, Russia

<sup>d</sup> Nikolaev Institute of Inorganic Chemistry SB RAS, 3 Lavrentyev Avenue, Novosibirsk 630090, Russia

<sup>e</sup> Novosibirsk State University, 1 Pirogov str., Novosibirsk 630090, Russia

## ARTICLE INFO

## Keywords:

Tin oxide  
Molecular-beam epitaxy  
X-ray phase analysis  
Raman spectroscopy  
X-ray photoelectron spectroscopy  
Morphology  
Refractive index  
Absorption edge  
Photoluminescence

## ABSTRACT

SnO and SnO<sub>2</sub> films were obtained on the SiO<sub>2</sub> surface by the molecular-beam epitaxy method. The initial films are in the polycrystalline phase. The annealing of SnO(x) films at a temperature of 300 °C resulted in the formation of the tetragonal SnO phase. Three vibration modes E<sub>g</sub>, A<sub>1g</sub>, and B<sub>1g</sub> with the frequencies of Sn–O bond vibrations of 113, 211 and ~360 cm<sup>-1</sup>, respectively, which correspond to the SnO phase, were first observed by the Raman spectroscopy method. The orthorhombic SnO<sub>2</sub> films were obtained by increasing the annealing temperature to 500 °C. Based on the valence band XPS (X-ray photoelectron spectroscopy) spectrum, several features with the binding energy approximately 5 eV, 7.5 eV and 11 eV, which are the same with the valence band of SnO<sub>2</sub>, were identified. The refractive index and absorption coefficient were investigated by the spectral ellipsometry technique. The high absorption coefficients correspond to the high Sn content. The film dielectric properties were revealed at the temperature higher than 300 °C. The refractive index values lie in the range of 1.5–2.6 for the visible spectral region. The pronounced absorption edges at 2.85 eV and 3.6 eV corresponding to those of stannous oxide (SnO) and stannic oxide (SnO<sub>2</sub>) were observed. The photoluminescence (PL) from the SnO(x) films was observed at room temperature. The increase of the annealing temperature resulted in the increase of PL intensity. Such PL intensity behavior is likely due to the Sn nanoislands.

## 1. Introduction

Metal oxides exhibit the properties of insulators, wide-gap semiconductors, metals, as well as superconductors [1]. Tin oxides belong to the class of materials that combine high electrical conductivity with the optical transparency in the visible range and are of interest as electrodes and buffer layers in solar cells [2], electroluminescent displays; they can be used in LEDs [3] and in other optoelectronic devices [4]. Doped tin oxides can be used in a large number of electronic devices (for example, in transparent field effect transistors [5–7]), as an alternative material to toxic and expensive CdO, ZnO or In<sub>2</sub>O<sub>3</sub>. Despite the fact that tin oxides are transparent in the visible range, they reflect the light in the infrared region of the electromagnetic spectrum. This property is important for the use of tin oxides in energy-saving devices. Architectural glass [8] coated with a tin oxide can transmit light, but

retain heat in a room. Other important applications of tin oxides include their use as solid state gas sensors [9,10] and the anode in lithium-ion batteries due to the reversibility of electrochemical reactions with lithium ions [11]. Basic tin oxides, such as SnO and SnO<sub>2</sub>, being semiconductors, have p- and n-type conductivities, respectively [12,13]. SnO<sub>2</sub> in its pure form is an n-type wide-gap semiconductor having the bandgap with direct transitions of 3.6 eV at room temperature [14]. Its electric conductivity is associated with oxygen vacancies and interstitial tin atoms. SnO<sub>2</sub> is one of the most widely used materials from the family of binary transparent conductive oxides [15]. The electron and optical properties of SnO<sub>2</sub> can greatly vary using dopants. For these purposes, for example, elements such as In, P, Sb, F are used [16]. A large number of deposition methods, such as electron beam evaporation [14], pulsed laser deposition [17], spray pyrolysis [18], vacuum evaporation [19], gas-phase deposition [20] and ion layering [21] are used

\* Corresponding author at: A.V. Rzhanov Institute of Semiconductor Physics SB RAS, 13 Lavrentyev Avenue, Novosibirsk 630090, Russia.

E-mail addresses: [nikif@isp.nsc.ru](mailto:nikif@isp.nsc.ru) (A. Nikiforov), [Vyacheslav.t@isp.nsc.ru](mailto:Vyacheslav.t@isp.nsc.ru) (V. Timofeev), [mash@isp.nsc.ru](mailto:mash@isp.nsc.ru) (V. Mashanov), [azarov\\_ivan@mail.ru](mailto:azarov_ivan@mail.ru) (I. Azarov), [idl@isp.nsc.ru](mailto:idl@isp.nsc.ru) (I. Loshkarev), [volodin@isp.nsc.ru](mailto:volodin@isp.nsc.ru) (V. Volodin), [gulyaev@isp.nsc.ru](mailto:gulyaev@isp.nsc.ru) (D. Gulyaev), [chia@catalysis.ru](mailto:chia@catalysis.ru) (I. Chetyrin), [korolkov@niic.nsc.ru](mailto:korolkov@niic.nsc.ru) (I. Korolkov).

<https://doi.org/10.1016/j.apsusc.2020.145735>

Received 7 October 2019; Received in revised form 10 January 2020; Accepted 10 February 2020

Available online 11 February 2020

0169-4332/ © 2020 Elsevier B.V. All rights reserved.

for the obtaining of homogeneous thin SnO<sub>2</sub> films. Another widely studied tin oxide is SnO, which has the p-type conductivity, mainly due to Sn vacancies and interstitial oxygen atoms [22]. The bandgap in SnO films varies from 2.5 to 3.4 eV [23]. Recently, a record mobility in SnO films has been obtained and thin-film transistors with p-type SnO films have been presented [23]. SnO films are prepared by various methods, such as electron beam evaporation [24], magnetron sputtering [25], sol-gel [26] and atomic layer deposition [27]. The structural, optical and electron SnO<sub>2</sub> and SnO film properties are affected by both their preparation conditions, and the formation technique. Despite a large number of studies on SnO (x) films, there are only a few reports on the formation of SnO and SnO<sub>2</sub> phases by molecular-beam epitaxy (MBE) [28,29]. The purpose of the article is to show the effect of annealing temperature on the morphology, phase composition and the optical properties of SnO(x) films obtained by MBE.

## 2. Experimental details

The SnO(x) film samples were obtained by the molecular-beam epitaxy (MBE) method. The MBE chamber was equipped with an electron-beam evaporator (EBE) for Si and an effusion cell for Sn. The Sn films were deposited on the Si substrate with a 100 nm thick SiO<sub>2</sub> layer at the Sn deposition rate of 0.28 Å/c in the presence of oxygen. The schematic structure of samples is demonstrated in Fig. 1. Molecular oxygen was supplied into the chamber through a leak. The Si EBE was used for the ionization of oxygen molecules. This process is to occur since the electrons created in the EBE have a high energy of about 5 keV. The initial base pressure in the MBE growth chamber was about 10<sup>-8</sup> Torr, whereas the process pressure during the growth was 10<sup>-6</sup> Torr. The substrate temperature was about 200 °C. After the Sn deposition, all samples were pulled out in the air and placed in a quartz tube. Further, they were annealed at the atmospheric pressure in the temperature range of 200–800 °C. The morphology and surface structure during the deposition in the MBE chamber was controlled by reflection high-energy electron diffraction (RHEED). The change of RHEED patterns allowed identifying the phase surface state of growing films. The crystalline structure and the phase analysis were performed by X-ray Powder Diffraction (XRPD), which presents a powder X-ray diffraction (XRD) system (Shimadzu XRD-7000, CuKα Radiation, λ = 1.54178 Å, linear detector OneSight) in the 2θ range from 10° to 65°. The indexing of diffraction patterns was carried out on the PDF database (Powder Diffraction File, released in 2010, International Center for Diffraction Data, Pennsylvania, USA). Raman spectroscopy for the structural analysis of SnO(x) films was used. The Raman spectra were obtained at room temperature under the excitation of an Ar laser line (514.5 nm) using a T64000 Horiba Jobin Yvon spectrometer with a micro-Raman setup. The spectrometer belongs to the Center of collective usage “VTAN” in Analytics and Technological Research Center of the Novosibirsk State University. The laser beam diameter and radiation power on the sample were 10 μm and 1 mW, respectively. There was no strong local heating of samples under these conditions. The spectral resolution was not worse than 2 cm<sup>-1</sup>. The scattered light polarization was not analyzed. Furthermore, the film morphology was analyzed by a scanning electron microscope (SEM) (Hitachi SU8220).

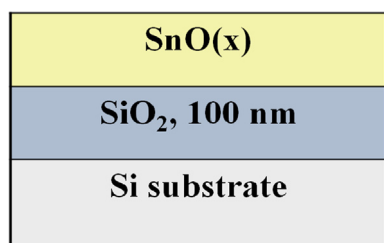


Fig. 1. Schematic structure of obtained samples with the SnO(x) film.

The SEM system allows carrying out the elemental analysis of the grown samples, since it additionally includes EDX (Energy-dispersive X-ray spectroscopy) Bruker detectors. The XFlash 5060F QUAD detector included in the SEM equipment was used for the analysis of the X-ray spectrum emission energy of the structures obtained by the MBE technique and annealed in the furnace. The analysis of the material chemical state, both in its initial state and after annealing, was carried out using a SPECS X-Ray photoelectron spectrometer (Germany). The spectrometer consists of three main vacuum chambers: a loading chamber, preparation chamber and an analyzer chamber equipped with manipulators for the samples transfer. The base pressure in the preparation chamber is  $5 \times 10^{-9}$  mbar and is maintained by a turbomolecular pump. The analyzer chamber is meant to record photoelectron spectra and is equipped with a hemispherical analyzer PHOIBOS-150-MCD-9, FOCUS-500 X-Ray monochromator and the XR-50 M X-Ray source with the double Al/Ag anode. The base pressure in the analyzer chamber is about  $5 \times 10^{-10}$  mbar. In this work, the characteristic monochromatic radiation AlK<sub>α1,2</sub> ( $h\nu = 1486.74$  eV, 200 W) was used to excite the spectra. The studies of optical constants in the wavelength range of 250–1000 nm were carried out by spectral ellipsometry. The measurements were made on the ellipsometers of our own design [30]. The film optical constants restoration included several steps. Firstly, the determination of the SiO<sub>2</sub> layer thickness and optical constants on the masked sample areas, where the SiO<sub>2</sub> sublayer was not covered by Sn, were made. Secondly, the determination of the SnO(x) layer thickness and optical constants was carried out. An independent solution of the inverse ellipsometry task was used at each stage for each wavelength with multi-angle spectral measurements (VASE). The film was considered uniform in depth. Therefore, the reconstructed dielectric functions and thickness are effective in case of a non-uniform layer structure. The processing on effective medium approximation (EMA) models and the recovery of dielectric SnO(x) cluster functions, after accumulating the sufficient amount of experimental data and comparing these dielectric functions with the microscopy data on the film morphology, are possible. The sample optical properties were studied by photoluminescence (PL) spectroscopy. To excite the PL, the HeCd laser with the wavelength of 325 nm and the excitation power of 2 mW was used. The PL was recorded by a spectrometer equipped with both a nitrogen-cooled silicon CCD matrix and a cooled photoelectron multiplier with an S-20 photocathode. The measurements were carried out at room temperature.

## 3. Results and discussion

The structural and optical properties of SnO(x) films were investigated. The Sn film was deposited on the Si substrate with a 100 nm thick SiO<sub>2</sub> layer at 200 °C. The oxygen flux was supplied into the MBE chamber during the Sn growth. The growing film morphology and surface structure were controlled in the growth process. The grown films were found to be polycrystalline. This conclusion can be made by the presence of rings on the RHEED patterns. After the growth in a vacuum chamber, the samples were unloaded and annealed at the atmospheric pressure. The annealing temperature was changed from 200 to 800 °C. To identify the crystalline structure, crystallite size and phase composition, it was necessary to apply the XRPD method. The X-ray phase analysis was made on the series of samples, which include the initial sample (as-grown) grown at 200 °C, as well as annealed samples. The XRD patterns for the as-grown sample, for the samples annealed at 200 and 300 °C as well as 500 and 600 °C, are demonstrated in Fig. 2. The range of angles  $2\theta = 28^{\circ}$ – $29^{\circ}$  from the measurements was excluded, since it contains an intense Si substrate peak. The calculated XRD patterns for Sn, SnO and SnO<sub>2</sub> material phases are also shown in Fig. 2 under the experimental XRD patterns. The as-grown sample diffraction peaks at  $2\theta = 30.6^{\circ}$ ,  $32.0^{\circ}$ ,  $43.9^{\circ}$  and  $44.9^{\circ}$  correspond to the (2 0 0), (1 0 1), (2 2 0) and (2 1 1) planes of the tetragonal Sn crystal (β-Sn, PDF #010-75-9188). Further, the SnO phase formation takes place

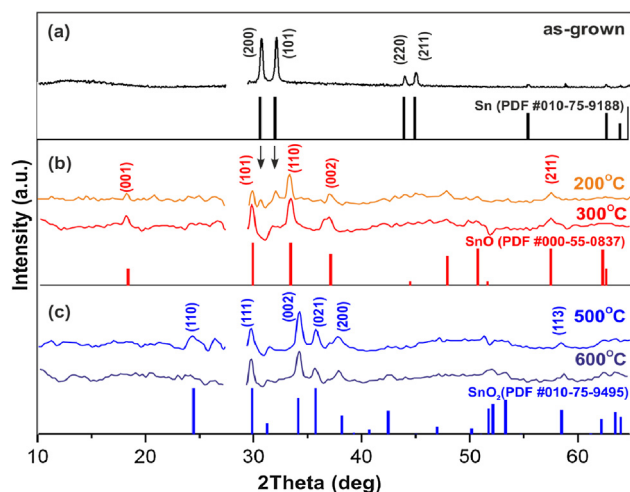


Fig. 2. Experimental XRD patterns of SnO(x) films: for the as-grown sample (a), for the annealed film at 200 and 300 °C (b) and at 500 and 600 °C, as well as the calculated XRD patterns of Sn, SnO and SnO<sub>2</sub> materials.

at the annealing temperature of 200 °C (Romarchite Tin Oxide, PDF # 000-55-0837), as shown in Fig. 2(b). Stannous tin oxide (SnO) is of tetragonal structure. However, the peaks, which correspond to β-Sn, still take place (these peaks are pointed out by the arrows). The temperature increase to 300 °C results in the single SnO phase formation. The phase transition to the crystalline film structure of stannic tin oxide (SnO<sub>2</sub>) is observed at 500 °C. The diffraction peaks at  $2\theta = 24.4^\circ, 29.9^\circ, 34.2^\circ, 35.8^\circ$  and  $38.2^\circ, 58.8^\circ$ , corresponding to the (1 1 0), (1 1 1), (0 0 2), (0 2 1), (2 0 0) and (1 1 3) planes of orthorhombic SnO<sub>2</sub> (o-SnO<sub>2</sub>, PDF #010-75-9495), are pointed out in Fig. 2 (c) for the sample annealed at 500 °C. The further temperature increase to 800 °C does not result in the change of the SnO<sub>2</sub> phase. However, the small tetragonal SnO<sub>2</sub> part was additionally appeared in the o-SnO<sub>2</sub> phase.

In order to carry out the structural analysis of SnO(x) films, Raman spectroscopy was used as well. The Raman spectra of both as-deposited and annealed SnO(x) films are shown in Fig. 3. The vertical scale is shown on the logarithmic scale for convenience. Since the films are semitransparent, the Raman signal originating from the Si substrate can be observed in the studied spectral region. The narrow peak at 520.6 cm<sup>-1</sup> appearing due to the scattering on long-wave optical phonons in monocrystalline Si can be seen in all spectra. For the first time, this peak was observed by Parker with coauthors [31]. This peak is seen even in the as-deposited film spectrum, but its intensity is relatively low; so, one can suppose that this film is less transparent. It can be due to presence of Sn clusters in the as-deposited film. The frequency of Sn-Sn bond vibrations in Sn clusters is about 200–210 cm<sup>-1</sup> (see [32] and references in it). However, one can see another feature with a position of approximately 114 cm<sup>-1</sup>. It is known that, in SnO, the Sn–O bonds have E<sub>g</sub>, A<sub>1g</sub> and B<sub>1g</sub> vibration modes with frequencies 113, 211 and 350–370 cm<sup>-1</sup>, respectively [33–38]. Therefore, it is not possible to clearly identify the presence of Sn-Sn bonds in the as-deposited film. But anyway, due to the fact that the film is barely transparent, one can assume that it contains Sn clusters that are highly light-absorbing. One can see a broad low-intensive band from 350 to 700 cm<sup>-1</sup> in the as-deposited film spectrum. It is known that in the monocrystalline rutile tin dioxide (SnO<sub>2</sub>), there are several Raman-active vibration modes with the frequencies from 313 to 774 cm<sup>-1</sup> [39]. It can be supposed that, in polycrystalline SnO(x) films, these modes can form a broad band.

One can see that the annealing at 200 °C leads to the growth of E<sub>g</sub> and A<sub>1g</sub> mode intensities and the appearance of a weak B<sub>1g</sub> mode. It can be due to the film oxidation of and SnO phase growth. There are also some features between E<sub>g</sub> (113 cm<sup>-1</sup>) and A<sub>1g</sub> (211 cm<sup>-1</sup>) modes. It can be due to the presence of the SnO(x) phase [34,37]. The low-

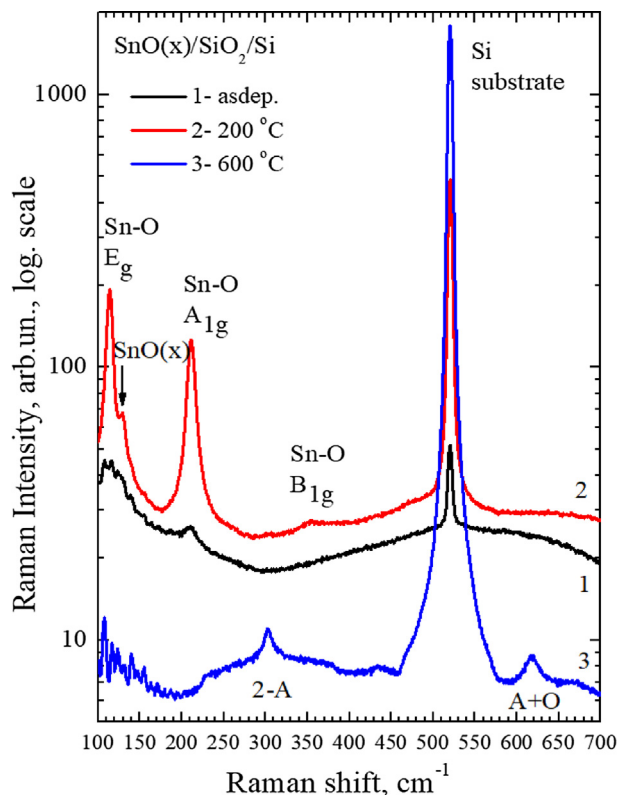
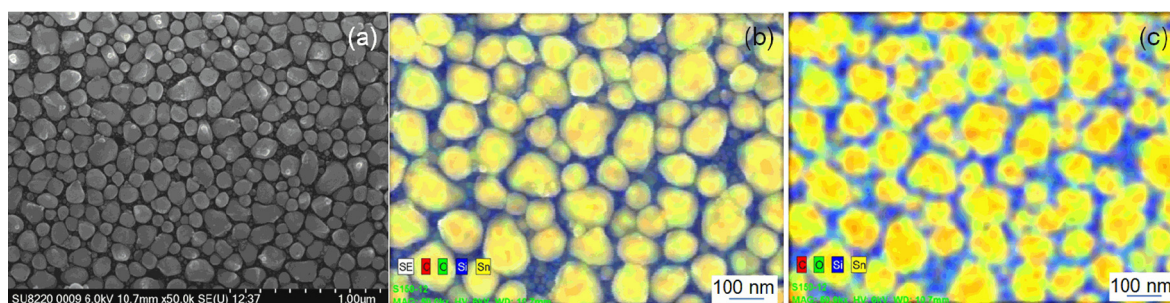


Fig. 3. Raman spectra of as-deposited and annealed SnO(x) films.

intensive feature at  $\sim 360$  cm<sup>-1</sup> can be associated with the B<sub>1g</sub> mode [38]. It should be noted that Guo and coauthors studied monocrystalline SnO [38]. We study thin films, but, nevertheless, we have some signal from the B<sub>1g</sub> mode. The subsequent annealing (600 °C) leads to a further film oxidation. One can see only the peculiarities between 200 and 450 cm<sup>-1</sup> and also the peak at 620 cm<sup>-1</sup>, which are due to the two-phonon scattering in the Si substrate [40,41].

The SEM technique was applied to observe the grown film morphology. The SEM images of the SnO(x) film at the annealing temperature of 400 °C are demonstrated in Fig. 4(a). Observing the SnO(x) film surface on the SEM image, one can see that the film is nanostructured. The elemental analysis of the samples was investigated by EDX spectroscopy, since the SEM system additionally includes the EDX detectors. The elemental distribution maps for the SnO(x) film are demonstrated in Fig. 4 (b) and (c). Fig. 4 (b) includes the data on the morphology, since the mapping for Sn, O, Si and C overlaps the information obtained from secondary electrons. The Sn, O and Si elements correspond to yellow, green and blue colors, respectively. The data of EDX analysis allow concluding that the islands are enriched by Sn and O, whereas the area between the islands contains the high Si content related to the Si substrate.

The study of the chemical state of SnO(x) films was performed by X-Ray photoelectron spectroscopy (XPS). The photoelectron spectra of the Sn3d<sub>5/2</sub> region for the initial sample (as-grown) and the sample annealed at 500 °C are shown in Fig. 5 (a) and (b), respectively. The decomposition of the Sn3d<sub>5/2</sub> region, shown in Fig. 5 (a), reveals the presence of peaks corresponding to different Sn oxidation degrees of 0 (metal), +2 (SnO) and +4 (SnO<sub>2</sub>). Since β-Sn, in the polycrystalline phase, takes place for the initial sample based on the results of the X-ray phase analysis, the SnO and SnO<sub>2</sub> phases obtained from the photoelectron spectra are in the amorphous state, and it arises due to the removal of samples into the ambient atmosphere. Therefore, this phase mixture was not identified in the XRPD method. The difference between the Sn<sup>2+</sup> state and Sn<sup>4+</sup> state equals about 0.9 eV. It is in good agreement with the result published in [42]. The analysis of Sn3d<sub>5/2</sub>



**Fig. 4.** The SEM image (a) and the map of elemental composition (b and c), obtained by energy dispersive X-ray (EDX) spectroscopy. Figure (b) includes the data on the morphology, since the mapping for Sn, O, Si and C overlaps the information obtained from secondary electrons. The Sn, O and Si elements correspond to yellow, green and blue colors, respectively.

photoelectron spectrum for the sample annealed at 500 °C demonstrates the existence of only single SnO<sub>2</sub> phase. Furthermore, the XPS survey spectra were recorded for series of samples. Besides the Sn peaks, O 1s and C 1s core level peaks were determined. Based on the survey scan, the separation between O 1s and Sn 3d<sub>5/2</sub> core level peaks was identified to be approximately 44 eV corresponding to the value obtained by Lau and Wertheim [43]. For further clarity, the analysis of valence band photoelectron spectra was performed. The valence band (VB) may be used for the determination of different phases present on the surface. The valence bands were successfully applied in [43] to elucidate the phase composition of tin oxide films. The valence band XPS spectrum for the SnO(x) film annealed at 500 °C is displayed in Fig. 6. This spectrum demonstrates the three main peaks, which are consistent with earlier XPS results [44]. The peaks appearing at about 5 eV are related to the O 2p level [44]. However, the peak in the region of 2–3 eV bound up with the mixing of Sn 5s and Sn 5p states, is not observed. The 5s-5p hybrid state was observed in the valence band XPS spectrum of SnO [45] or SnO<sub>2</sub>, which is oxygen depleted. The states around 7.5 eV are attributed to the Sn 5p orbitals hybridized with O 2p orbitals, whereas the peak observed at about 11 eV is due to the Sn 5s – O 2p interacting orbitals [45]. Thereby, it was shown that these three features are the fingerprints of SnO<sub>2</sub>. Furthermore, the valence band XPS spectrum allows restoring the band structure of the investigated material. Since the tail is observed in the bulk bandgap of Fig. 6 in the range of 0–3 eV, it is necessary to identify the exact position of the valence-band edge. Based on a simple extrapolation technique, the valence-band edge equals about 3.2 eV binding energy relative to the Fermi level of the spectrometer. Knowing the material bandgap and the electron work function from the metal with which the sample is in contact, one can determine the electron affinity. These data will be useful, in the future.

The optical constants of the obtained SnO(x) film were studied by spectral ellipsometry. The refractive index for the initial sample and

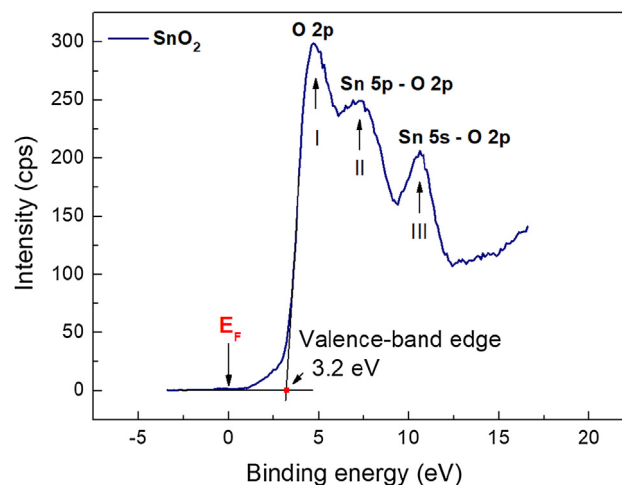


**Fig. 6.** Valence band XPS spectrum of the SnO<sub>2</sub> thin film. The linear extrapolation of the valence-band edge is shown.

several annealed samples are shown in Fig. 7(a). The anomalous dispersion type, which is characteristic for metals with high absorption values in the entire visible range, and a sharp course of the refractive index curve are observed. This indicates the presence of high Sn content in the film in the metal phase. Tin is oxidized at the temperature increase, and the transition to the normal dispersion occurs to the typical refractive index values for dielectrics at the level of 1.5–2.6 for the visible part of the spectrum. This is consistent with the published data on tin oxides [46]. A characteristic absorption incidence in the region of 3.6 eV is observed for the high-temperature annealing at 700 °C (Fig. 7 (b)), which can be related to the SnO<sub>2</sub> bandgap. The absorption edge

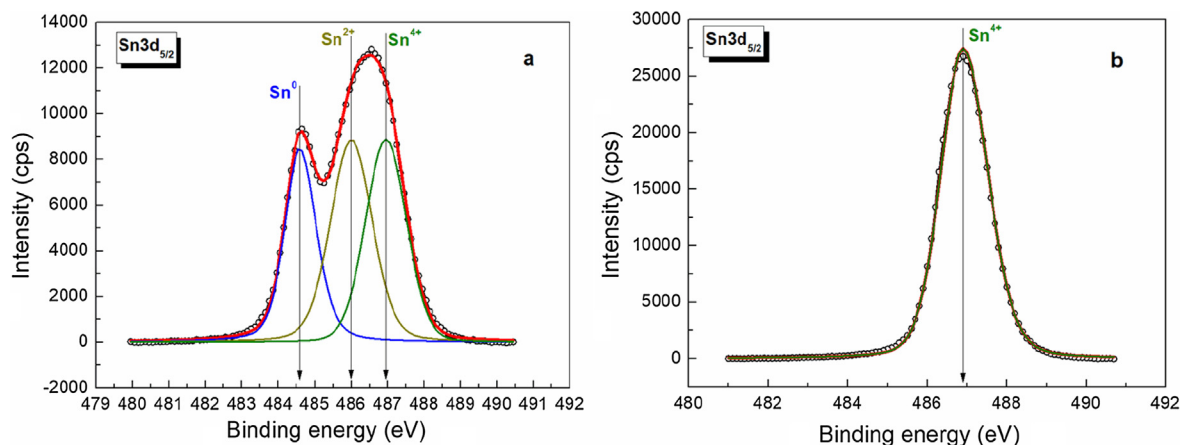


**Fig. 5.** Photoelectron spectra of the Sn 3d<sub>5/2</sub> regions for the as-grown sample (a) and for the sample annealed at 500 °C (b).

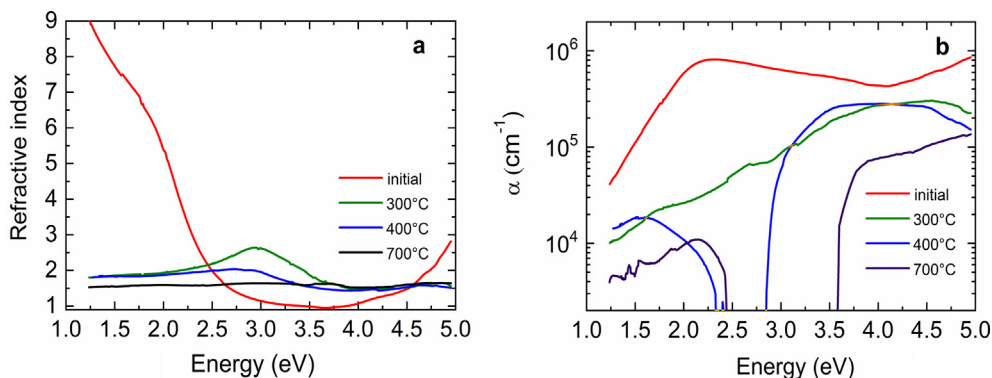


Fig. 7. Refractive index dependences on the energy at the annealing temperature increase (a) and the absorption coefficient dependencies against the energy at the annealing temperature increase (b).

shifts toward lower energies at lower annealing temperatures. It is observed at 2.85 eV for the annealing temperature of 400 °C. Taking into account [47], it can be concluded that the stannous oxide (SnO) is formed at this temperature. By the way, the results of X-ray phase analysis confirm this inference as well. The edge becomes unexpressed with the characteristic incidences in the regions of 2 eV and 2.6 eV at the annealing temperature of 300 °C. These values point out the critical points for the SnO(x) structure, where x, according to other methods, is close to 1. According to [37], the monoxide bandgap is varied in the region of 2.35–2.47 eV, which is close to the value of 2.6 eV observed in our case.

The optical properties of SnO(x) films were studied by photoluminescence (PL) spectroscopy. The PL spectra obtained from the SnO (x) films demonstrated in Fig. 8. The numbers in Fig. 8(a) indicate the spectra corresponding to several annealing temperatures. A wide PL region is observed in the range 450–850 nm with a PL maximum at about 600 nm. A similar PL was observed in the case of SnO<sub>2</sub> nanoribbons obtained by laser ablation [48] and SnO<sub>2</sub> nanorods synthesized from a solution [49]. Usually, the PL in this range is associated with crystal defects or defective levels that appear during a film growth or annealing. Defective levels are expected to be created by either oxygen vacancies or interstitial tin atoms. The increase in the annealing temperature from 500 °C to 800 °C leads to an almost 6-fold intensity increase. As shown in Fig. 7(b), the visible absorption was associated with the small concentration of Sn crystallites. Therefore, the rise of the PL intensity with the annealing temperature increase can occur as a result of a further film oxidation and the formation of Sn islands of several nanometers in diameter, which contribute to the radiative recombination. Moreover, if the electron emission current in the electron-beam

evaporator is increased from 50 mA to 65 mA, the elevation of the PL intensity is observed by a factor of 2 (Fig. 8(b)). The increase in the electron emission current should increase the oxygen ionization and, hence, the oxidized part of the initial film. Thus, the cluster size surrounded by the oxide matrix and obtained in the case of higher emission current values decreases faster during the annealing. They make a larger contribution to the PL increase, as shown in Fig. 8(b).

#### 4. Conclusion

The SnO and SnO<sub>2</sub> films were obtained on the SiO<sub>2</sub> surface by the Sn deposition from a molecular beam in the oxygen flux. The initial films are in the polycrystalline phase, as shown by the reflection high-energy electron diffraction technique during the film deposition by MBE. The annealing of SnO(x) films at the temperature of 300 °C resulted in the formation of the tetragonal SnO phase (romarchite tin oxide). It was demonstrated by the x-ray phase analysis. Three vibration modes E<sub>g</sub>, A<sub>1g</sub>, and B<sub>1g</sub> with the frequencies of Sn–O bond vibrations 113, 211 and ~360 cm<sup>-1</sup>, respectively, which correspond to the SnO phase, were first observed by the Raman spectroscopy method. The annealing temperature increase to 500 °C created the orthorhombic SnO<sub>2</sub> phase. The analysis of the Sn3d<sub>5/2</sub> photoelectron spectrum for the annealed sample at 500 °C demonstrates the existence of only single SnO<sub>2</sub> phase. Furthermore, three features on the valence band XPS spectrum with the binding energy approximately 5 eV, 7.5 eV and 11 eV, which are fingerprints of SnO<sub>2</sub>, were shown. The optical properties of the SnO(x) films were studied by the ellipsometry and photoluminescence methods before and after the annealing in the atmosphere in the temperature range of 200–800 °C. The high absorption coefficients correspond to the

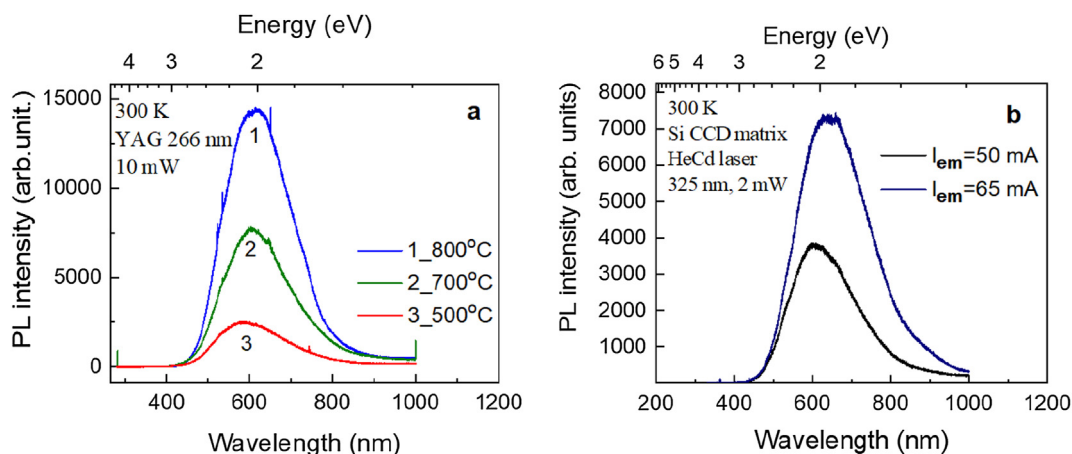


Fig. 8. Photoluminescence spectra: (a) from the sample annealing at the different temperatures; (b) from samples annealed at 800 °C and grown the different emission currents.

high metallic Sn content. The film dielectric properties appear at the annealing temperature increase. The refractive index values for dielectrics at the level of 1.5–2.6 for the visible region of the spectrum were obtained. The pronounced absorption edge in the visual range at 2.85 eV, corresponding to the stannous oxide (SnO), was observed for the annealing temperature of 400 °C. The absorption edge shifts to 3.6 eV at the temperature of 700 °C. This value is in a good agreement with the literature data on the SnO<sub>2</sub> bandgap. The PL spectra were obtained from the SnO (x) films at room temperature. The annealing temperature increase from 500 °C to 800 °C results in the PL intensity increase. The PL intensity rise with the annealing temperature increase can be related to the Sn nanoislands.

### CRedit authorship contribution statement

**A. Nikiforov:** Conceptualization. **V. Timofeev:** Investigation. **V. Mashanov:** Writing - original draft. **I. Azarov:** Software. **I. Loshkarev:** Investigation. **V. Volodin:** Investigation. **D. Gulyaev:** Investigation. **I. Chetyrin:** Investigation. **I. Korolkov:** Investigation.

### Acknowledgements

This work was supported by the Russian Foundation for Basic Research, grant No. 18-32-20064, 18-42-540018, 18-52-41006. The SEM investigations and EDX analysis were carried out with the help of the “Nanostructures” Collective-Use Center. The authors are grateful to Center of collective usage “VTAN” in Analytics and Technological Research Center “High Technology and Nanostructured Materials” of NSU. The work was partly carried out according to the ISP SB RAS state research programs, project No. 0306-2019-0019 (Raman studies of the samples). The authors would like to thank Tatyana GavriloVA for her SEM investigations and EDX analysis.

### Declaration of Competing Interest

The authors declare that they have no competing interests.

### References

- P.-J. Chen, H.-T. Jeng, Phase diagram of the layered oxide SnO: GW and electron-phonon studies, *Sci. Rep.* 5 (2015) 16359, <https://doi.org/10.1038/srep16359>.
- M.A. Hossain, J.R. Jennings, Z.Y. Koh, Q. Wang, Carrier generation and collection in CdS/CdSe-sensitized SnO<sub>2</sub> solar cells exhibiting unprecedented photocurrent densities, *ACS Nano* 5 (2011) 3172–3181, <https://doi.org/10.1021/nn200315b>.
- Y. Li, W. Yin, R. Deng, R. Chen, J. Chen, Q. Yan, B. Yao, H. Sun, S.-H. Wei, T. Wu, Realizing a SnO<sub>2</sub>-based ultraviolet light-emitting diode via breaking the dipole-forbidden rule, *NPG Asia Mater.* 4 (2012) e30, <https://doi.org/10.1038/am.2012.56>.
- X. Yu, T.J. Marks, A. Facchetti, Metal oxides for optoelectronic applications, *Nat. Mater.* 15 (2012) 383–396, <https://doi.org/10.1038/NMAT4599>.
- R.E. Presley, C.L. Munsee, C.-H. Park, D. Hong, J.F. Wager, D.A. Keszler, Tin oxide transparent thin-film transistors, *J. Phys. D Appl. Phys.* 37 (2004) 2810–2813, <https://doi.org/10.1088/0022-3727/37/20/006>.
- K.J. Saji, K. Tian, M. Snure, A. Tiwari, 2D tin monoxide - an unexplored p-Type van der Waals semiconductor: material characteristics and field effect transistors, *Adv. Electron. Mater.* 2 (2016) 1500453, <https://doi.org/10.1002/aelm.201500453>.
- E. Fortunato, P. Barquinha, R. Martins, Oxide semiconductor thin-film transistors: a review of recent advances, *Adv. Mater.* 24 (2012) 2945–2986, <https://doi.org/10.1002/adma.201103228>.
- M. Batzill, U. Diebold, The surface and materials science of tin oxide, *Prog. Surf. Sci.* 79 (2005) 47–154, <https://doi.org/10.1016/j.progsurf.2005.09.002>.
- D. Nunes, A. Pimentel, A. Gonçalves, S. Pereira, R. Branquinho, P. Barquinha, E. Fortunato, R. Martins, Metal oxide nanostructures for sensor applications, *Semicond. Sci. Technol.* 34 (2019) 043001, <https://doi.org/10.1088/1361-6641/ab011e>.
- A. Palacios-Padros, M. Altomare, A. Tighineanu, R. Kirchgorg, N.K. Shrestha, I. Diez-Perez, F. Caballero-Briones, F. Sanz, P. Schmuki, Growth of ordered anodic SnO<sub>2</sub> nanochannel layers and their use for H<sub>2</sub> gas sensing, *J. Mater. Chem. A* 2 (2014) 915–920, <https://doi.org/10.1021/acs.chemmater.6b03952>.
- N. Mohri, B. Oschmann, F. Mueller, J. von Zamory, N. laszczynski, M. N. Tahir, S. Passerini, R. Zentel, W. Tremel, Synthesis and characterization of carbon coated sponge-like tin oxide (SnOx) films and their application as electrode materials in lithium-ion batteries, *J. Mater. Chem. A* 4 (2016) 61–619, <http://doi.org/10.1039/C5TA06546A>.
- J.P. Allen, D.O. Scanlon, S.C. Parker, G.W. Watson, Tin Monoxide: Structural Prediction from First Principles Calculations with van der Waals Corrections, *J. Phys. Chem. C* 115 (2011) 19916–19924, <https://doi.org/10.1021/jp205148y>.
- Z. Galazka, R. Uecker, D. Klimm, K. Irmscher, M. Pietsch, R. Schewski, M. Albrecht, A. Kwasiński, S. Ganschow, D. Schulz, C. Guguschev, R. Bertram, M. Bickermann, R. Fornari, Growth, characterization, and properties of bulk SnO<sub>2</sub> single crystals, *Phys. Status Solidi A* 211 (2014) 66–73, <https://doi.org/10.1002/pssa.201330020>.
- A.F. Khan, M. Mehmood, M. Aslam, M. Ashraf, Characteristics of electron beam evaporated nanocrystalline SnO<sub>2</sub> thin films annealed in air, *Appl. Surf. Sci.* 256 (2010) 2252–2258, <https://doi.org/10.1016/j.apsusc.2009.10.047>.
- D. Ginley, H. Hosono, D.C. Paine, *Handbook of Transparent Conductors*, Springer, US, Boston, 2010.
- T. Tesfamichael, G. Will, M. Colella, J. Bell, Optical and electrical properties of nitrogen ion implanted fluorine doped tin oxide films, *Nucl. Instr. Meth. Phys. Res. B* 201 (2003) 581–588, [https://doi.org/10.1016/S0168-583X\(02\)02226-7](https://doi.org/10.1016/S0168-583X(02)02226-7).
- C. Ristoscu, L. Cultrera, A. Dima, A. Perrone, R. Cutting, H.L. Du, A. Busiakiewicz, Z. Klusek, P.K. Datta, S.R. Rose, SnO<sub>2</sub> nanostructured films obtained by pulsed laser ablation deposition, *Appl. Surf. Sci.* 247 (2005) 95–100, <https://doi.org/10.1016/j.apsusc.2005.01.171>.
- K.S. Shamala, L.C.S. Murthy, K. Narasimha Rao, Studies on tin oxide films prepared by electron beam evaporation and spray pyrolysis methods, *Bull. Mater. Sci.* 27 (2004) 295–301, <https://doi.org/10.1007/BF02708520>.
- Y.-N. Nuli, S.-L. Zhao, Q.-Z. Qin, Nanocrystalline tin oxides and nickel oxide film anodes for Li-ion batteries, *J. Power Sources* 114 (2003) 113–120, [https://doi.org/10.1016/S0378-7753\(02\)00531-1](https://doi.org/10.1016/S0378-7753(02)00531-1).
- P. Duverneuil, F. Maury, N. Peberé, F. Senocq, H. Vergnes, Chemical vapor deposition of SnO<sub>2</sub> coatings on Ti plates for the preparation of electrocatalytic anodes, *J. Surf. Coat. Technol.* 151–152 (2002) 9–13, [https://doi.org/10.1016/S0257-8972\(01\)01618-8](https://doi.org/10.1016/S0257-8972(01)01618-8).
- S.N. Pusawale, P.R. Deshmukh, C.D. Lokhande, Chemical synthesis and characterization of hydrous tin oxide (SnO<sub>2</sub>·H<sub>2</sub>O) thin films, *Bull. Mater. Sci.* 34 (2011) 1179–1183, <https://doi.org/10.1007/s12034-011-0168-3>.
- A. Togo, F. Oba, K. Tatsumi, First-principles calculations of native defects in tin monoxide, *Phys. Rev. B* 74 (2006) 195128, <https://doi.org/10.1103/PhysRevB.74.195128>.
- R. Sivaramasubramaniam, M.R. Muhamad, S. Radhakrishna, Optical properties of annealed Tin(II) oxide in different ambients, *Phys. Status Solidi A* 136 (1993) 215, <https://doi.org/10.1002/pssa.2211360126>.
- L.Y. Liang, Z.M. Liu, H.T. Cao, X.Q. Pan, Microstructural, optical, and electrical properties of SnO thin films prepared on quartz via a two-step method, *ACS Appl. Mater. Interfaces* 2 (2010) 1060, <https://doi.org/10.1021/am900838z>.
- H. Yabuta, N. Kaji, R. Hayashi, H. Kumomi, K. Nomura, T. Kamiya, M. Hirano, H. Hosono, Sputtering Formation of p-Type SnO Thin-Film Transistors on Glass Toward Oxide Complimentary Circuits, *Appl. Phys. Lett.* 97 (2010) 072111, <https://doi.org/10.1063/1.3478213>.
- M. Marikkannan, V. Vishnukanthan, A. Vijayshankar, J. Mayandi, J.M. Pearce, A novel synthesis of tin oxide thin films by the sol-gel process for optoelectronic applications, *AIP Adv.* 5 (2015) 027122, <https://doi.org/10.1063/1.4909542>.
- X. Du, Y. Du, S.M. George, In situ examination of tin oxide atomic layer deposition using quartz crystal microbalance and Fourier transform infrared techniques, *J. Vac. Sci. Technol. A* 23 (2005) 581, <https://doi.org/10.1116/1.1914810>.
- M. Batzill, J.M. Burst, U. Diebold, Pure and cobalt-doped SnO<sub>2</sub>(101) films grown by molecular beam epitaxy on Al<sub>2</sub>O<sub>3</sub>, *Thin Solid Films* 484 (2005) 132–139, <https://doi.org/10.1016/j.tsf.2005.02.016>.
- S.K.V. Farahani, T.D. Veal, J.J. Mudd, D.O. Scanlon, G.W. Watson, O. Bierwagen, M.E. White, J.S. Speck, C.F. McConville, Valence-band density of states and surface electron accumulation in epitaxial SnO<sub>2</sub> films, *Phys. Rev. B* 90 (2014) 155413, <https://doi.org/10.1103/PhysRevB.90.155413>.
- E.V. Spesivtsev, S.V. Rykhlitskii, V.A. Shvets, Development of methods and instruments for optical ellipsometry at the Institute of Semiconductor Physics of the Siberian Branch of the Russian Academy of Sciences, *Optoelectron. Instrum. Data Process.* 47 (2011) 419–425, <https://doi.org/10.3103/S8756699011050219>.
- J.H. Parker Jr., D.W. Feldman, M. Ashkin, Raman scattering by silicon and germanium, *Phys. Rev.* 155 (1967) 712–714, <https://doi.org/10.1103/PhysRev.155.712>.
- V.A. Volodin, V.A. Timofeev, A.I. Nikiforov, M. Stoffel, H. Rinnert, M. Vergnat, Vibrational and light-emitting properties of Si/Si<sub>1-x</sub>Sn<sub>x</sub> heterostructures, *JETP Lett.* 109 (2019) 368–371, <https://doi.org/10.1134/S0370274X19060055>.
- J. Geurts, S. Rau, W. Richter, F.J. Schmitte, SnO films and their oxidation to SnO<sub>2</sub>: Raman scattering, IR reflectivity and X-ray diffraction studies, *Thin Solid Films* 121 (1984) 217–225, [https://doi.org/10.1016/0040-6090\(84\)90303-1](https://doi.org/10.1016/0040-6090(84)90303-1).
- L. Sangaletti, L.E. Depero, B. Allieri, F. Pioselli, E. Comini, G. Sberveglieri, M. Zocchi, Raman Oxidation of Sn Thin Films to SnO<sub>2</sub>. Micro-Raman Mapping and X-ray Diffraction Studies, *J. Mater. Res.* 13 (1998) 2457–2460, <http://doi.org/10.1557/JMR.1998.0343>.
- S. Koval, R. Burriel, M.G. Stachiotti, M. Castro, R.L. Migoni, M.S. Moreno, A. Varela, C.O. Rodriguez, Linear augmented-plane-wave frozen-phonon calculation, shell-model lattice dynamics, and specific-heat measurement of SnO, *Phys. Rev. B* 60 (1999) 14496–14499, <https://doi.org/10.1103/PhysRevB.60.14496>.
- H. Luo, L.Y. Liang, H.T. Cao, Z.M. Liu, F. Zhuge, Structural, chemical, optical, and electrical evolution of SnOx films deposited by reactive RF magnetron sputtering, *ACS Appl. Mater. Interfaces* 4 (2012) 5673–5677, <https://doi.org/10.1021/am301601s>.
- Y.A. El-Gendy, Effects of film thickness on the linear and nonlinear refractive index of p-type SnO films deposited by e-beam evaporation process, *Physica B* 526 (2017) 59–63, <https://doi.org/10.1016/j.physb.2017.06.006>.

- [38] Y.Q. Guo, R.Q. Tan, X. Li, J.H. Zhao, Z.L. Luo, C. Gao, W.J. Song, Shape-controlled growth and single-crystal XRD study of submillimeter-sized single crystals of SnO, *CrystEngComm* 13 (2011) 5677–5680, <https://doi.org/10.1039/C0CE00949K>.
- [39] S.H. Sun, G.W. Meng, G.X. Zhang, T. Gao, B.Y. Geng, L.D. Zhang, J. Zuo, Raman scattering study of rutile SnO<sub>2</sub> nanobelts synthesized by thermal evaporation of Sn powders, *Chem. Phys. Lett.* 376 (2003) 103–107, [https://doi.org/10.1016/S0009-2614\(03\)00965-5](https://doi.org/10.1016/S0009-2614(03)00965-5).
- [40] A.V. Kolobov, Raman scattering from Ge nanostructures grown on Si substrates: power and limitations, *J. Appl. Phys.* 87 (2000) 2926, <https://doi.org/10.1063/1.372279>.
- [41] A.I. Yakimov, A.V. Dvurechenskii, V.A. Volodin, M.D. Efremov, A.I. Nikiforov, G.Yu. Mikhalyov, E.I. Gatskevich, G.D. Ivlev, Effect of pulsed laser action on hole-energy spectrum of Ge/Si self-assembled quantum dots, *Phys. Rev. B* 72 (2005) 115318, <https://doi.org/10.1103/PhysRevB.72.115318>.
- [42] F.A. Akgul, C. Gumus, A.O. Er, A.H. Farha, G. Akgul, Y. Ufuktepe, Z. Liu, Structural and electronic properties of SnO<sub>2</sub>, *J. Alloy. Compd.* 579 (2013) 50–56, <https://doi.org/10.1016/j.jallcom.2013.05.057>.
- [43] C.L. Lau, G.K. Wertheim, Oxidation of tin: An ESCA study, *J. Vacuum Sci. Technol.* 15 (1978) 622, <https://doi.org/10.1116/1.569642>.
- [44] K. Nose, A.Y. Suzuki, N. Oda, M. Kamiko, Y. Mitsuda, Oxidation of SnO to SnO<sub>2</sub> thin films in boiling water at atmospheric pressure, *Appl. Phys. Lett.* 104 (2014) 091905, <https://doi.org/10.1063/1.4867654>.
- [45] P. De Padova, R. Larciprete, C. Ottaviani, C. Quaresima, P. Perfetti, E. Borsella, C. Astaldi, C. Comicioli, C. Crotti, M. Matteucci, M. Zacchigna, K. Prince, Synchrotron radiation photoelectron spectroscopy of the O(2s) core level as a tool for monitoring the reducing effects of ion bombardment on SnO<sub>2</sub> thin films, *Appl. Surf. Sci.* 104 (105) (1996) 349–353, [https://doi.org/10.1016/S0169-4332\(96\)00169-9](https://doi.org/10.1016/S0169-4332(96)00169-9).
- [46] S. Goldsmith, E. Cetinorgu, R.L. Boxman, Modeling the optical properties of tin oxide thin films, *Thin Solid Films* 517 (2009) 5146–5150, <https://doi.org/10.1016/j.tsf.2009.03.019>.
- [47] W. Guo, L. Fu, Y. Zhang, K. Zhang, L.Y. Liang, Z.M. Liu, H.T. Cao, X.Q. Pan, Microstructure, optical, and electrical properties of p-type SnO thin films, *Appl. Phys. Lett.* 96 (2010) 042113, <https://doi.org/10.1063/1.3277153>.
- [48] J.Q. Hu, Y. Bando, Q.L. Liu, D. Golberg, Laser-Ablation growth and optical properties of wide and long single-crystal SnO<sub>2</sub> ribbons, *Adv. Func. Mater.* 13 (2003) 493–496, <https://doi.org/10.1002/adfm.200304327>.
- [49] B. Cheng, J.M. Russell, W. Shi, L. Zhang, E.T. Samulski, Large-Scale, solution-phase growth of single-crystalline SnO<sub>2</sub> nanorods, *J. Am. Chem. Soc.* 126 (2004) 5972, <https://doi.org/10.1021/ja0493244>.